

# **Reversible Adsorption with Oriented Arrangement of Zwitterionic Additive Stabilizes Electrodes for Ultralong-Life Zn-Ion Batteries**

Huaming Yu<sup>1</sup>, Dongping Chen<sup>1</sup>, Xuyan Ni<sup>1</sup>, Piao Qing<sup>1</sup>, Chunshuang Yan<sup>3</sup>, Weifeng Wei<sup>1</sup>, Jianmin Ma<sup>2</sup>, Xiaobo Ji<sup>1</sup>, Yuejiao Chen<sup>1\*</sup>, Libao Chen<sup>1\*</sup>

<sup>1</sup>State Key Laboratory of Powder Metallurgy, Central South University, Changsha 410083, P. R. China

<sup>2</sup>School of Chemistry, Tiangong University, Tianjin 300387, P. R. China

<sup>3</sup>MIIT Key Laboratory of Critical Materials Technology for New Energy Conversion and Storage, School of Chemistry and Chemical Engineering, Harbin Institute of Technology, Harbin, 150001, P. R. China

## **Experimental Section**

### **Material synthesis**

The L-CN/ZnSO<sub>4</sub> electrolytes were prepared by adding pure L-Carnitine (L-CN) into 2 M ZnSO<sub>4</sub> solution at room temperature. L-Carnitine (98%) and Betaine (98%) were purchased from Macklin. V<sub>2</sub>O<sub>5</sub> was purchased from Aladdin. The Zn foils (99.99%) were purchased from Sinopharm.

### **Material Characterization**

The SEM and transmission electron microscope measurements were carried out on TESCAN MIRA to characterize the morphology of samples. The crystal structure and material composition information were gathered by XPS (Thermo Scientific K-Alpha), the Fourier transform infrared (FT-IR) (Thermo Scientific iN10) and <sup>1</sup>H magnetic resonance imaging (NMR) spectroscopy (Bruker Avance NEO 400MHz). X-ray diffraction (XRD) (EmpyrenE, PANalytical) was used to analyze the crystalline structures in the scanning range between 5° and 80° (2θ) with a step size of 0.02°. 2D Raman mapping on the surfaces of Zn electrodes and Raman intensity change maps during Zn deposition were obtained by In Situ Raman Spectroscopy (Thermo Scientific DXR3). The H<sub>2</sub> evolution was quantified by in-situ electrochemical-gas chromatography (EC-GC). The interface morphologies of symmetric cells with zinc electrodes during Zn plating process at 5 mA cm<sup>-2</sup> were observed by the optical microscope (DMM-900c, Caikon) with HD camera (CK-500, Caikon). The confocal laser scanning microscope (CLSM) images were obtained by the 3D Laser Scanning Confocal Microscope (VK-X1000, KEYENCE CORPORATION OF CHINA) to construct surface topographies. The Zeta potential was collected on a Zeta potential analyzer (Malvern Zetasizer Nano ZS90). The Zn/Ti cell was disassembled after discharging 1 h at the current density of 1 mA cm<sup>-2</sup>, took out the Ti electrode, and collected the deposited Zn metal on the Ti electrode to test the Zeta potential.

### **Electrochemical Characterization**

The Zn//Zn symmetric cells were assembled in the CR2025 coin cells in an air atmosphere. A glass fiber filter (Whatman) was used as separator. Galvanostatic charge/discharge curves, rate performance and long-term cycling tests were recorded on a NEWARE battery-testing instrument (Shenzhen, China) at different current densities at 25°C. The EIS spectra (from 100 kHz to 0.1 Hz), CV, Linear polarization

curves and chronoamperometry (CA) were tested on an electrochemical workstation (Ivium, Netherlands). According to the previous report, the EDLC value was calculated by the equation of  $C=i/v$  (C: capacitance, i: current. i was defined by half of the difference between positive and negative scanning current at each scanning rate). The full cells were cycled in the voltage range of 0.4-1.4 V. Typically, the  $V_2O_5$ , carbon black and polyvinylidene fluoride (PVDF) were mixed in N-methyl pyrrolidone solvent at a weight ratio of 7:2:1 to obtain a slurry. The obtained slurry was coated on titanium steel foil (20  $\mu\text{m}$ ) and dried at 80  $^\circ\text{C}$  for 12 h. The mass loadings of active material were about 1.2  $\text{mg cm}^{-2}$ .

### Simulation Method

The molecular dynamics simulations were performed using the GRMOACS 2020.6 package. The Visualization of structures were performed by VMD software. The molecular were mixed in a cubic box with periodic boundary conditions by using PACKMOL package. The number of the molecular is shown in the table:

system	H <sub>2</sub> O	ZnSO <sub>4</sub>	Betaine	L-CN
H <sub>2</sub> O	13889	500	\	\
Betaine	13889	500	3	\
L-CN	13889	500	\	3

The Generation Amber Force Field (GAFF) was selected in this work, which is good for investigation of various small organic molecules. The ACPYPE code was used to generate the desired force field parameters for the simulation systems. The partial charges on atoms were obtained using restrained electrostatic potential (RESP) method which calculated with Multiwfn software.

Before starting MD simulation, the initial configurations were relaxed using a conjugate gradient minimization scheme. The step size was 0.01 nm, and the cycle was set to 5000 steps. The minimization was considered to have converged when the minimum force was less than 100  $\text{kJ}\cdot\text{mol}^{-1}\cdot\text{nm}^{-1}$ . The van der Waals interaction was calculated by the cut-off method, atomic electrostatic interaction was calculated by PME (particle mesh Ewald), and both the cut-off and PME distances were 1.0 nm. Then, the system was equilibrated with a pressure of 1.0 bar to achieve a desired density. The Berendsen and V-rescale methods were used to control the pressure and

temperature. The time constant was 1.0 ps, and the compressibility was  $4.5 \times 10^{-5} \text{ bar}^{-1}$ . The equilibrium was 5 ns for all systems with a 0.001 ps time step. Finally, the production ran for 50 ns. The pressure control was changed to the Parrinello-Rahman method in the production run. In addition, the LINCS (Linear Constrain Solver) algorithm was used to impose constraints on the hydrogen bond.

Binding Energies and desolvation energies were conducted in Gaussian (G09) program at B3LYP-D3(BJ)/6-311+G(d,p) level. The implicit universal solvation model based on Solute Electron Density (SMD) with a dielectric constant of water was employed to investigate the influence of solvent. The binding energies ( $E_B$ ) were calculated by the following equation:

$$E_B = E_{com} - \sum E_{fra}$$

where  $E_{com}$  is the total energy of the complex,  $E_{fra}$  is the energy of each fragment. The desolvation energies ( $E_{des}$ ) were calculated by

$$E_{des} = E_{s2} + E_{sol} - E_{s1}$$

where  $E_{s1}$  and  $E_{s2}$  are the total energies of the solvation structures before and after desolvation, and  $E_{sol}$  is the energy of the solvent.

The calculation related to the interaction between Zn crystal and molecules were performed by DMol3 code in Material Studio software, with Perdew-Burke-Ernzerhof (PBE) generalized gradient approximation (GGA) and double-numerical properties plus polarization (DNP) functions as base set. In the convergence tolerance, the energy, force, and displacement were set as  $10^{-6}$  Ha,  $0.004 \text{ Ha}/\text{\AA}$ , and  $0.005 \text{ \AA}$ , separately. To avoid the influence of periodic adjacent layers, a vacuum layer of  $15 \text{ \AA}$  was used in the direction of vertical substrate plane. The absorbed energy between Zn slab and different molecules was defined as following equation:

$$E_{aborb} = E_{Zn-slab + molecules} + E_{Zn-slab} - E_{molecules}$$

## Results and Discussion

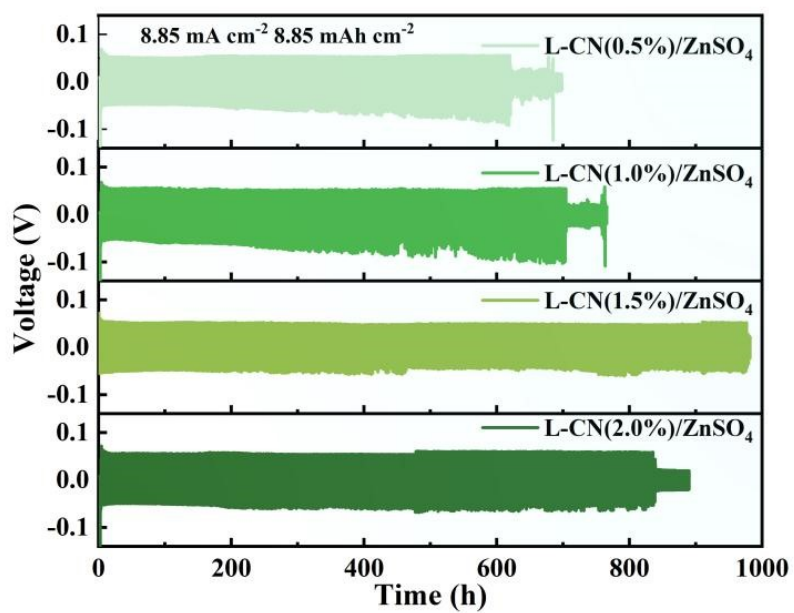


**Figure S1.** Long-term galvanostatic cycling performance of Zn//Zn symmetrical batteries in electrolytes with different concentrations of L-CN.

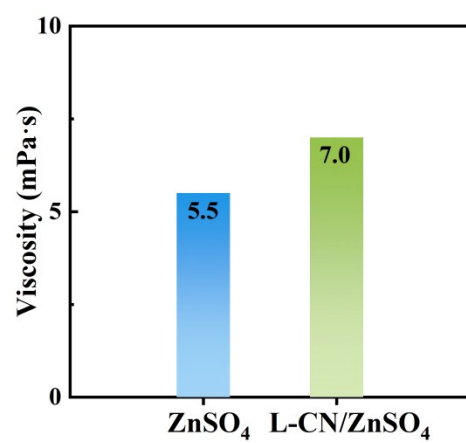


**Figure S2.** The viscosity of aqueous electrolytes with/without L-CN additive.

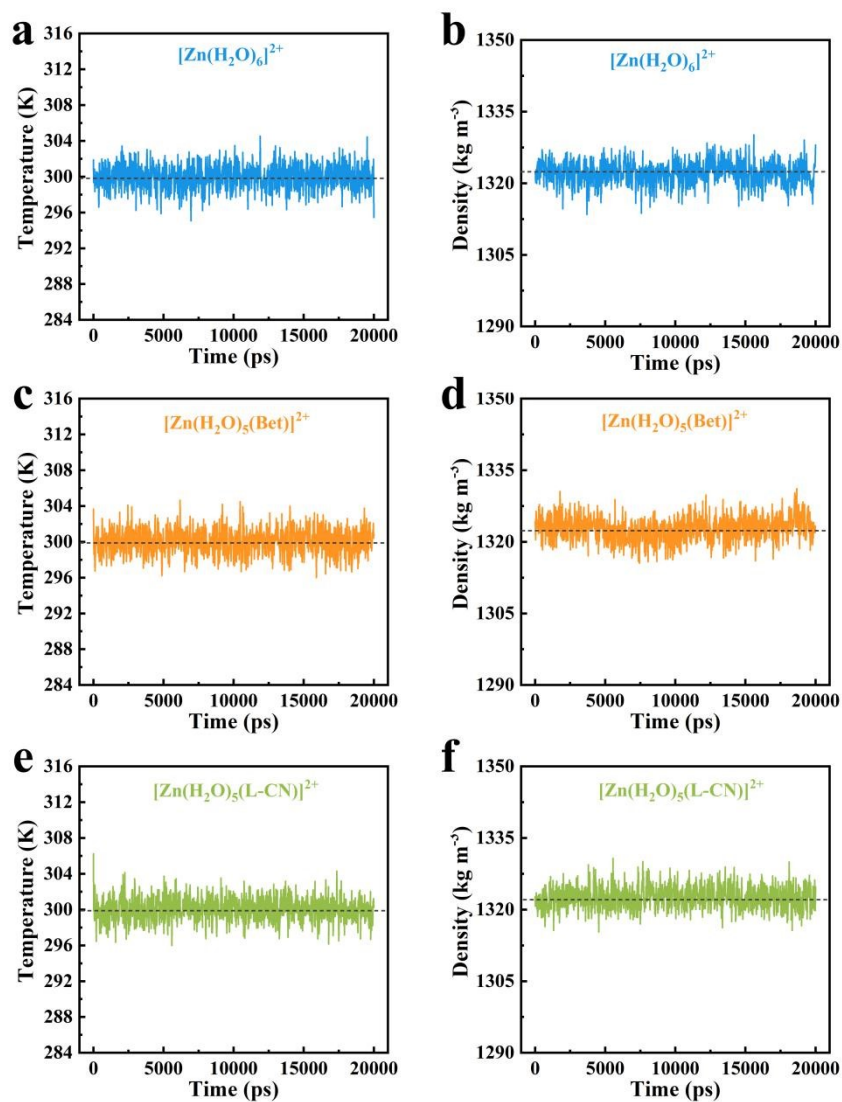


**Figure S3.** The time versus temperature curves in electrolyte systems: (a)  $\text{ZnSO}_4$ , (c)  $\text{ZnSO}_4\text{-Bet}$  and (e)  $\text{ZnSO}_4\text{-L-CN}$ . The time versus density curves: (b)  $\text{ZnSO}_4$  system, (d)  $\text{ZnSO}_4\text{-Bet}$  system and (f)  $\text{ZnSO}_4\text{-L-CN}$  system.

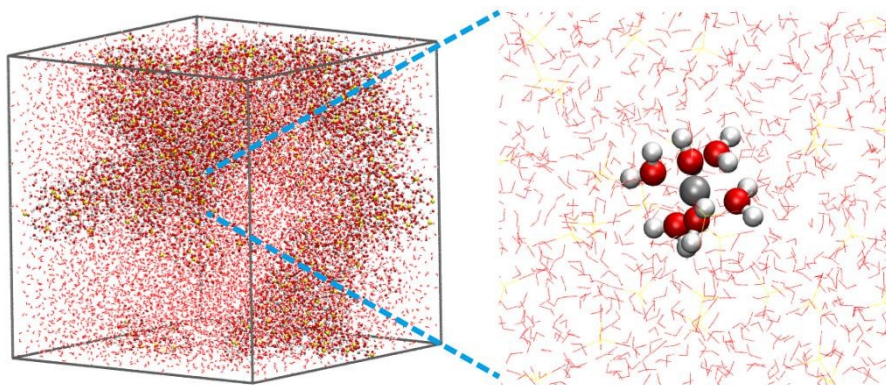


**Figure S4.** Snapshot of  $\text{ZnSO}_4$  electrolyte system obtained from MD simulation, and the partial enlarged snapshot representing  $\text{Zn}^{2+}$  solvation structure.

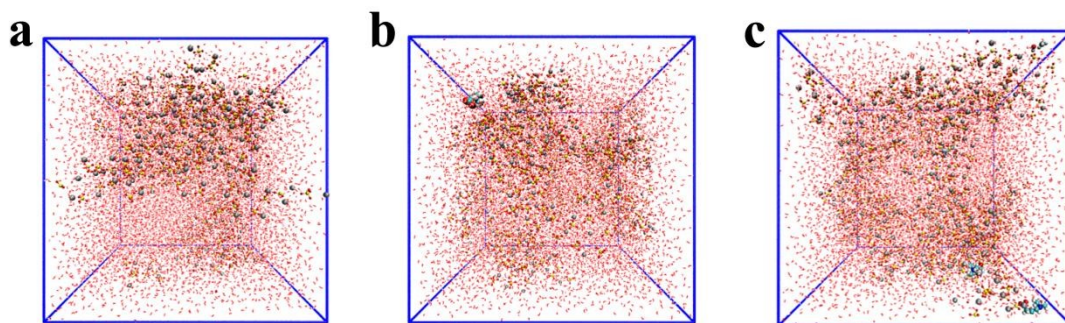


**Figure 5.** Snapshot of  $\text{ZnSO}_4$ ,  $\text{ZnSO}_4$ -Bet and  $\text{ZnSO}_4$ -L-CN systems obtained from MD simulation.

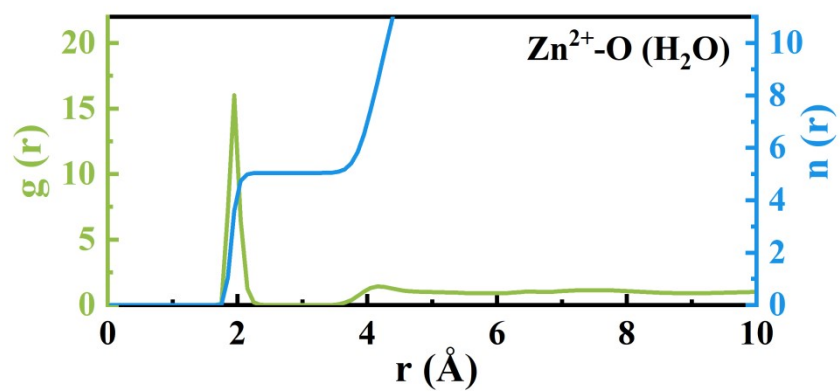


**Figure S6.** RDFs for Zn<sup>2+</sup>-O (H<sub>2</sub>O) and the coordination number in pure ZnSO<sub>4</sub> electrolyte.

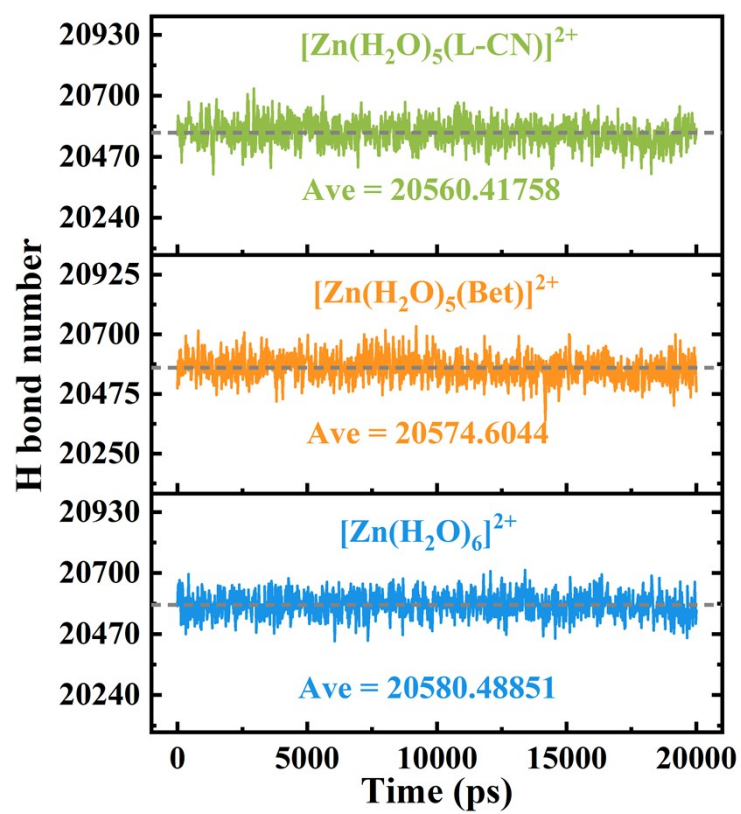


**Figure S7.** Number counts for hydrogen-bonds inside pure  $\text{ZnSO}_4$ ,  $\text{Bet}/\text{ZnSO}_4$  and (e)  $\text{L-CN}/\text{ZnSO}_4$  electrolytes.

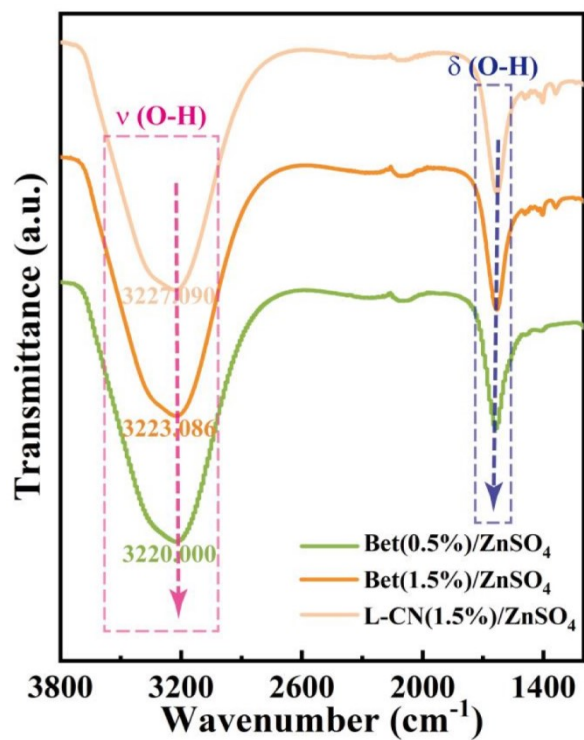


**Figure S8.** FTIR spectra of the electrolytes containing different concentrations of Bet and L-CN.

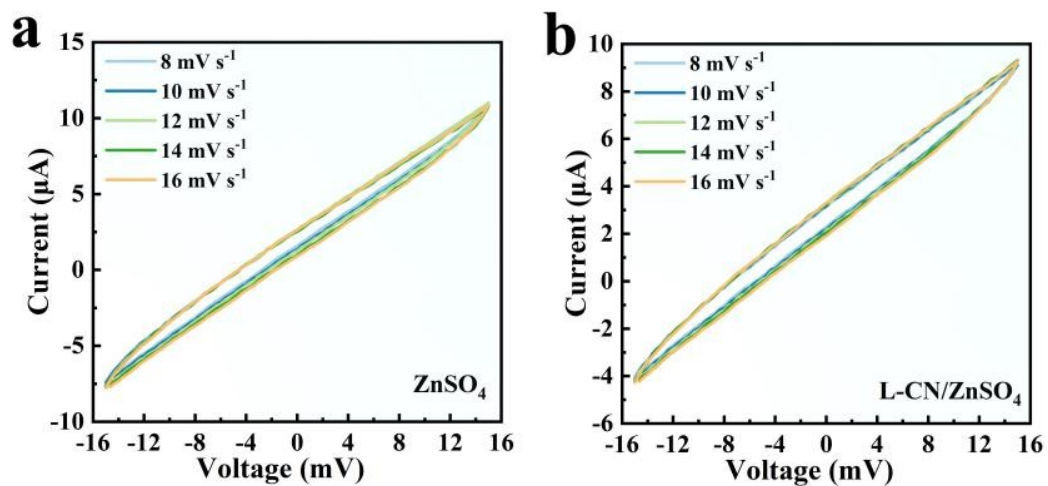


**Figure S9.** Electric double layer capacitance measurements for Zn substrates in 1 M  $\text{ZnSO}_4$  electrolytes with and without L-CN additive. Cyclic voltammograms curves for Zn-Zn symmetric coin cells in a voltage range from -15 mV to 15 mV under various scanning rates.

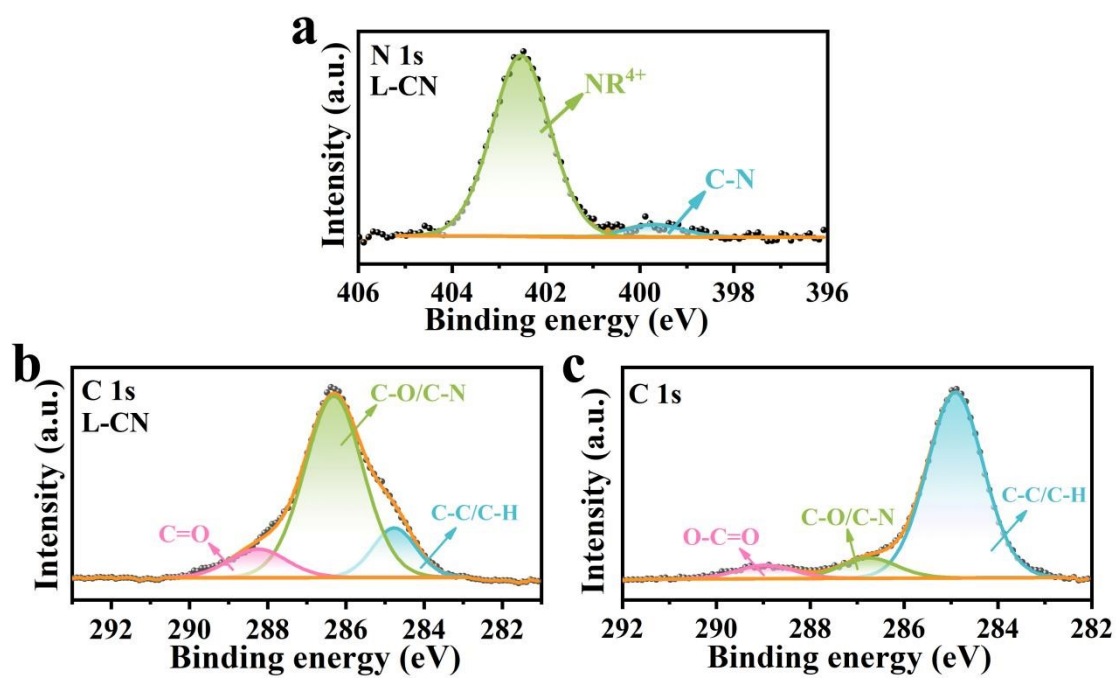


**Figure S10.** (a) N 1s and (b) C 1s XPS spectra of L-CN. (c) C 1s XPS spectra of Zn anode after 50 cycles in L-CN/ZnSO<sub>4</sub> electrolyte.

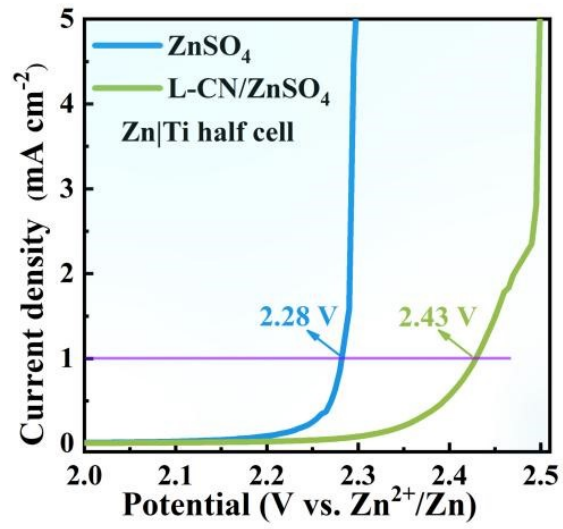


**Figure S11.** The linear sweep voltammetry curves of Zn/Ti half cells tested in L-CN/ZnSO<sub>4</sub> and ZnSO<sub>4</sub> electrolyte.

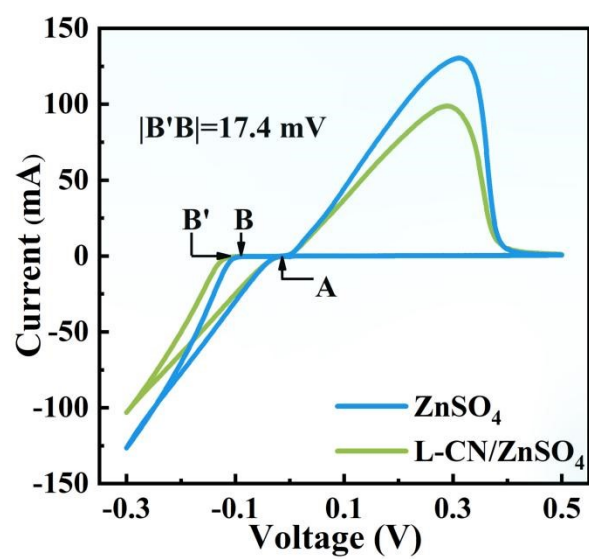


**Figure S12.** CV profiles for the Zn nucleation on Ti foil in L-CN/ZnSO<sub>4</sub> and ZnSO<sub>4</sub> electrolyte at 1.0 mV s<sup>-1</sup>.

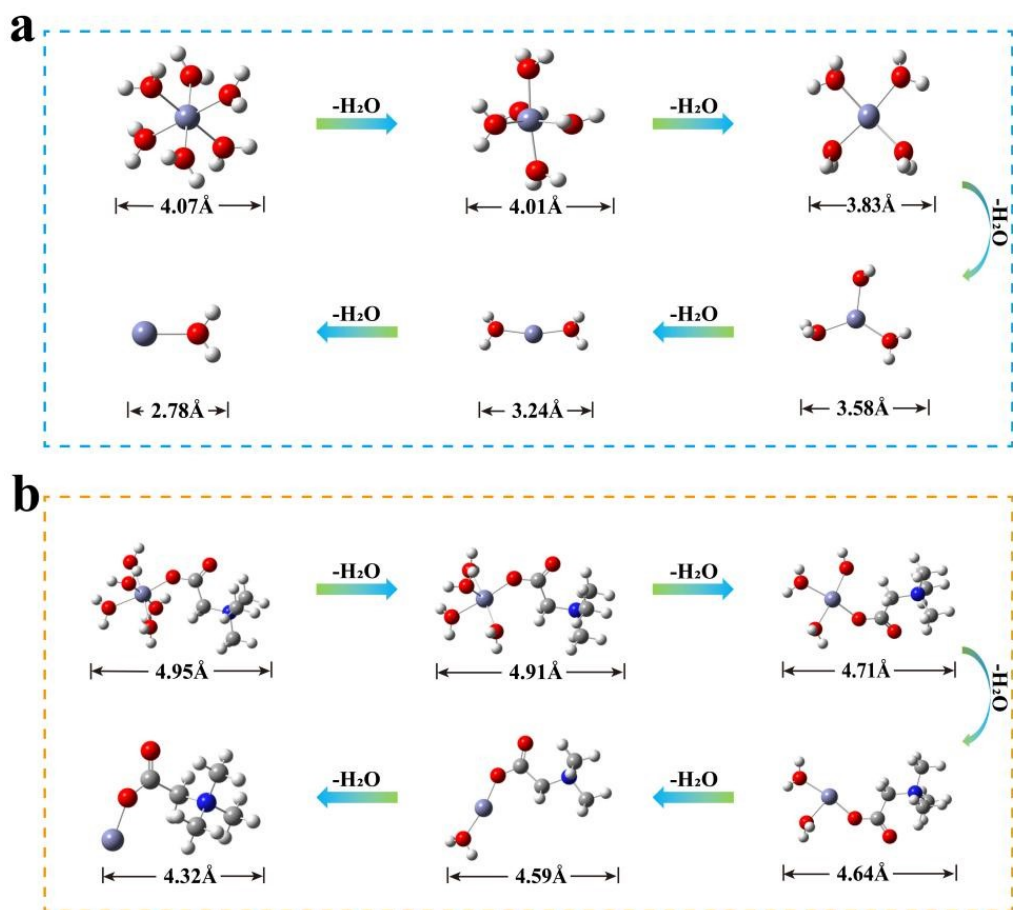


**Figure S13.** The molecular geometries of the desolvation processes for  $[(\text{Zn}(\text{H}_2\text{O})_{6-x})]^{2+}$  ( $x=1-6$ ) and  $[(\text{Zn}(\text{H}_2\text{O})_{5-x}(\text{Bet}))]^{2+}$  ( $x=1-5$ ) complexes.

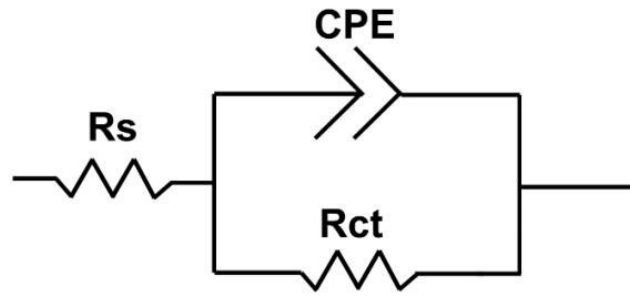


**Figure S14.** Fitting circuit of symmetric batteries.

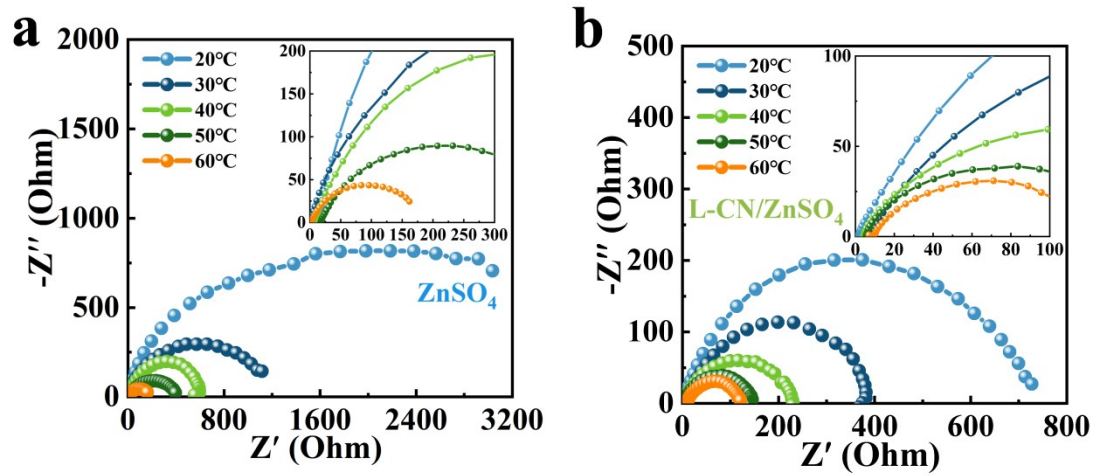


**Figure S15.** Nyquist plots at different temperatures for Zn//Zn symmetrical batteries in pure ZnSO<sub>4</sub> and L-CN/ZnSO<sub>4</sub> electrolytes.

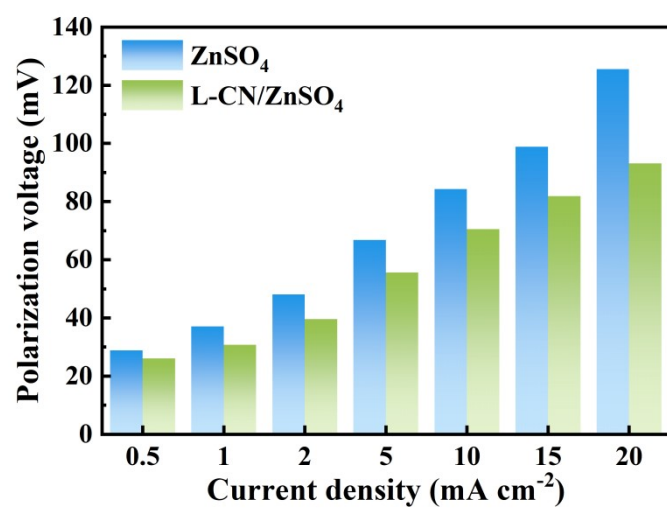


**Figure S16.** Polarization voltage values at different current densities.

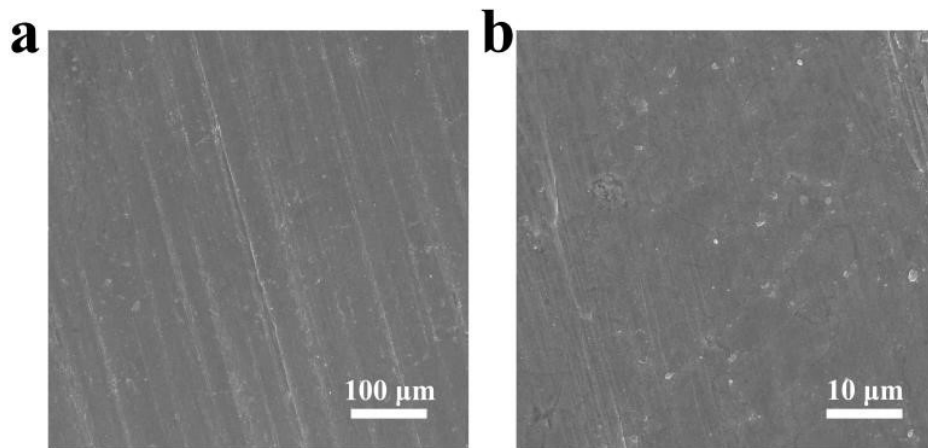


**Figure S17.** SEM images of pure Zn sheet.

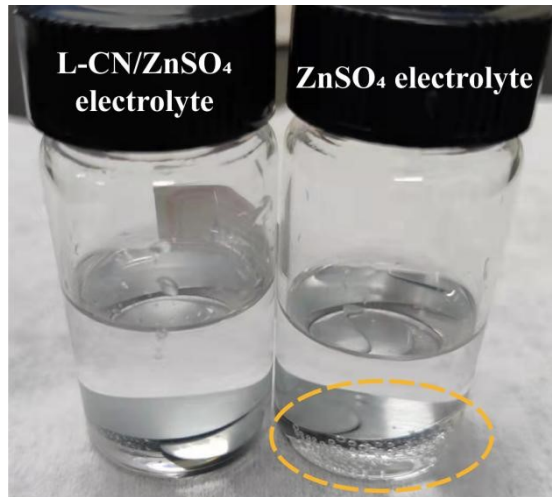


**Figure S18.** Optical images of the Zn foil immersed in electrolytes with/without L-CN.

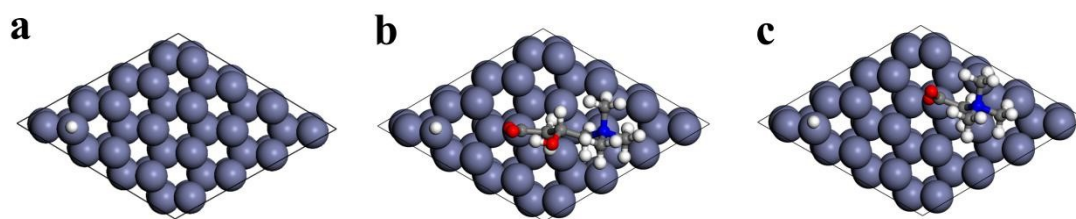


**Figure S19.** The corresponding adsorbed models for the hydrogen barrier of pure ZnSO<sub>4</sub>, bet/ZnSO<sub>4</sub> and L-CN/ZnSO<sub>4</sub> electrolytes.

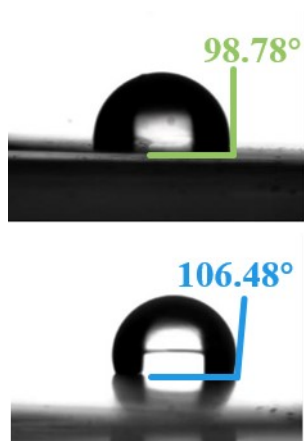


**Figure S20.** Contact angles of pure  $\text{ZnSO}_4$  (bottom) and L-CN/ $\text{ZnSO}_4$  (top) electrolytes on the Zn electrode.

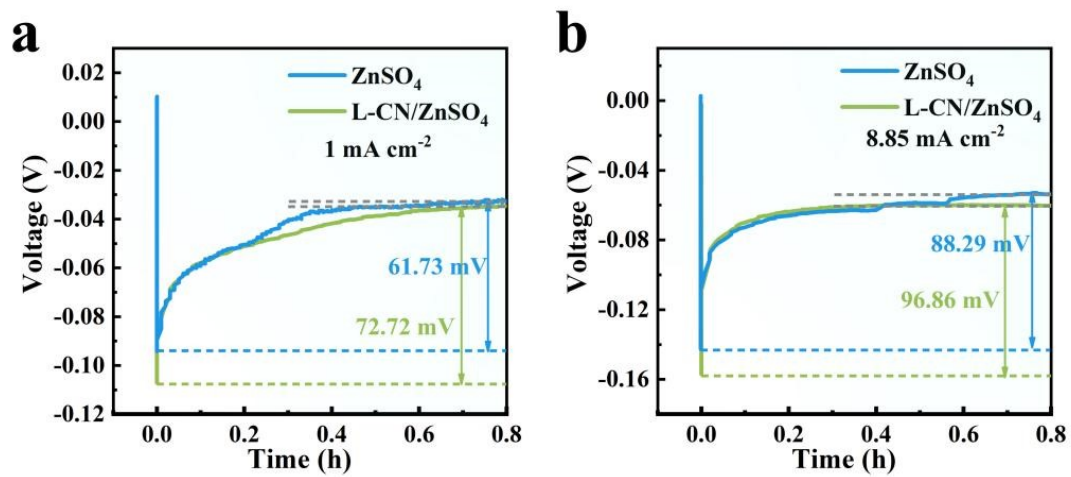


**Figure S21.** The nucleation overpotential tested in L-CN/ZnSO<sub>4</sub> and pure ZnSO<sub>4</sub> electrolytes at different current densities.

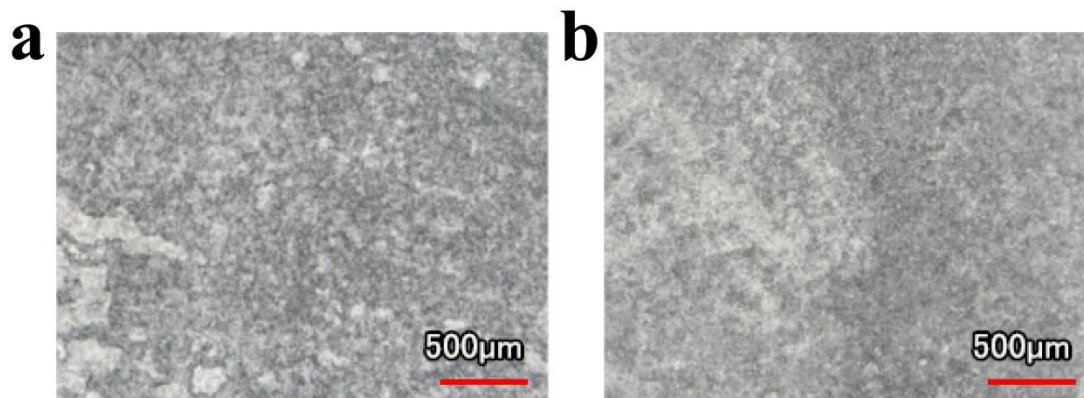


**Figure S22.** LSM images with the corresponding surface roughness curve on Zn anodes after 50 cycles in pure  $\text{ZnSO}_4$  electrolyte (left) and L-CN/ $\text{ZnSO}_4$  electrolyte (right).

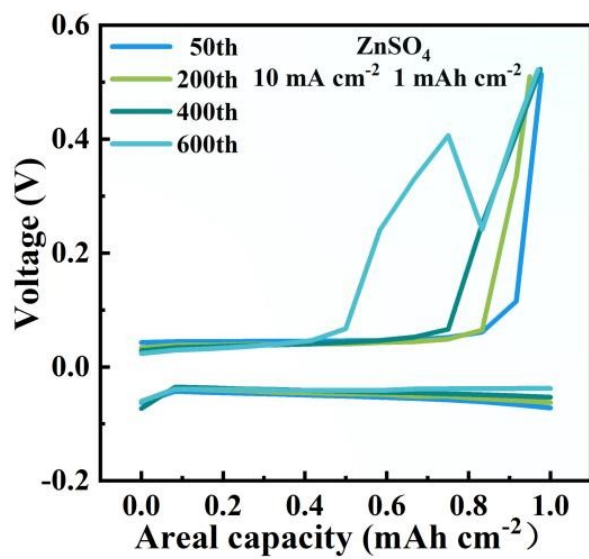


**Figure S23.** The corresponding voltage profiles at various cycles on Ti in pure  $\text{ZnSO}_4$  electrolyte.

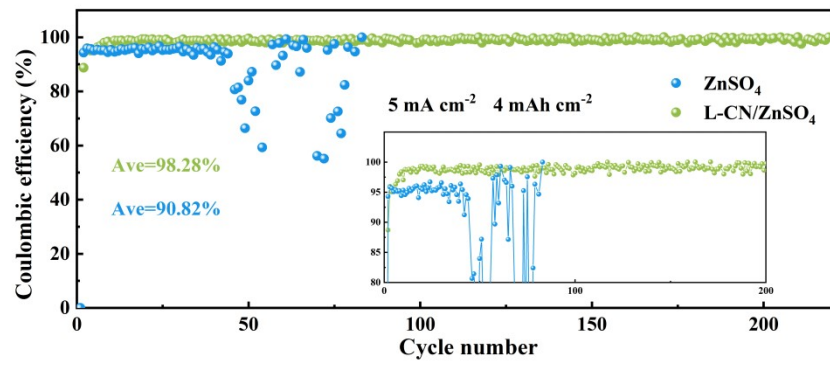


**Figure S24.** Zn Coulombic efficiency of Zn/Ti cells and in electrolytes with/without L-CN additive.

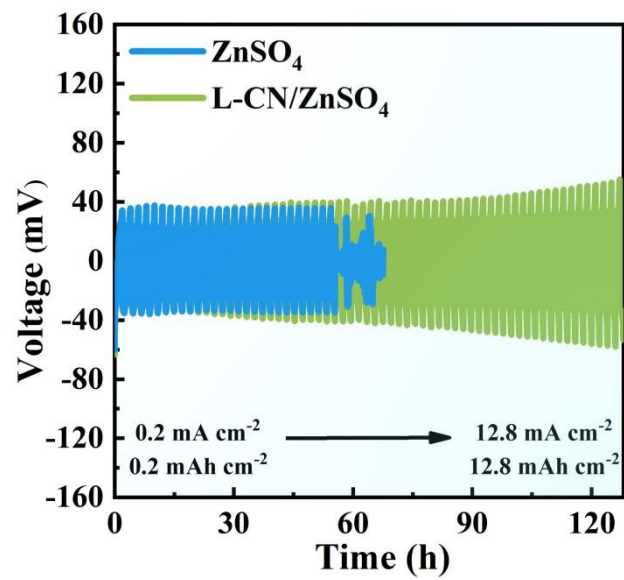


**Figure S25.** Potential evolution of symmetric cells at step-increased current densities.

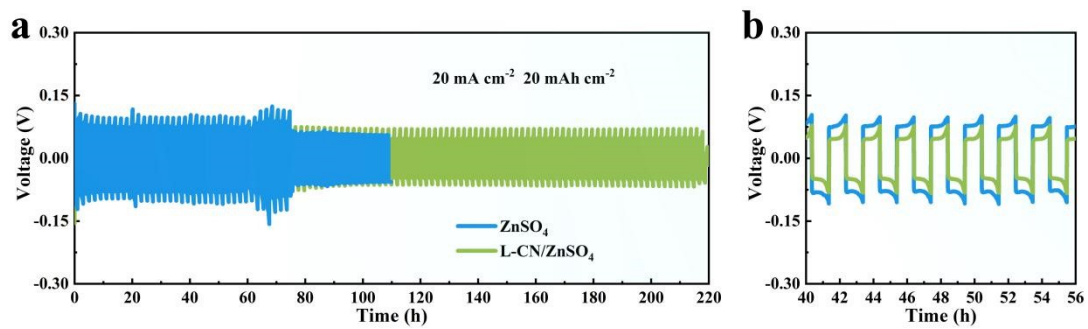


**Figure S26.** Long-term galvanostatic cycling performance of Zn//Zn symmetrical batteries in electrolytes with/without L-CN additive ( $20 \text{ mA cm}^{-2}$  with  $20 \text{ mAh cm}^{-2}$ ).

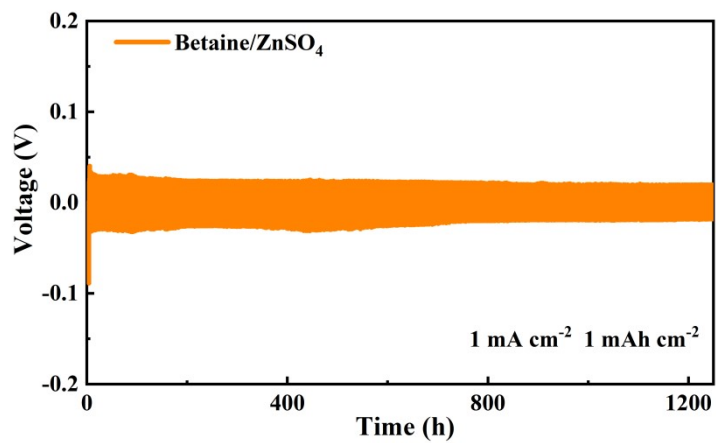


**Figure S27.** Long-term galvanostatic cycling performance of Zn//Zn symmetrical batteries in Bet/ZnSO<sub>4</sub> electrolyte.

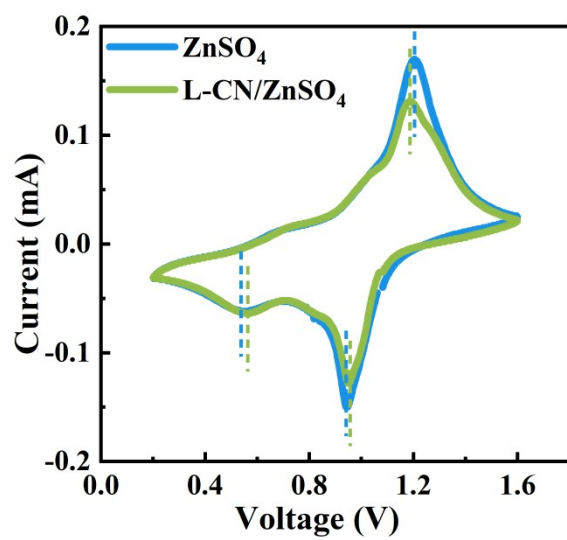


**Figure S28.** Cyclic voltammetry curves of Zn//V<sub>2</sub>O<sub>5</sub> full cells in electrolytes with/without L-CN additive at a scan rate of 0.1 mV s<sup>-1</sup>.

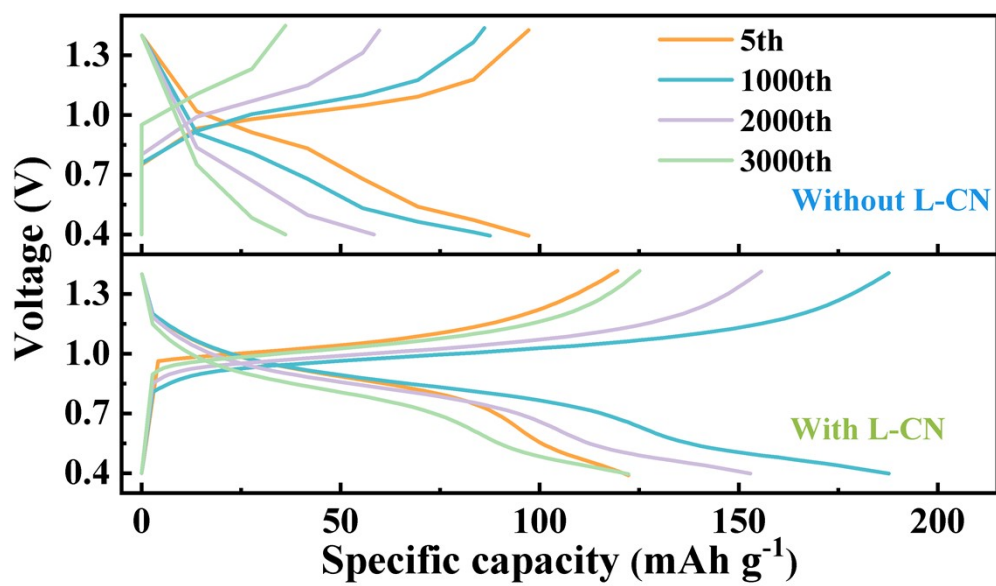


**Figure S29.** Corresponding charging/discharging curve in electrolytes with/without L-CN additive.

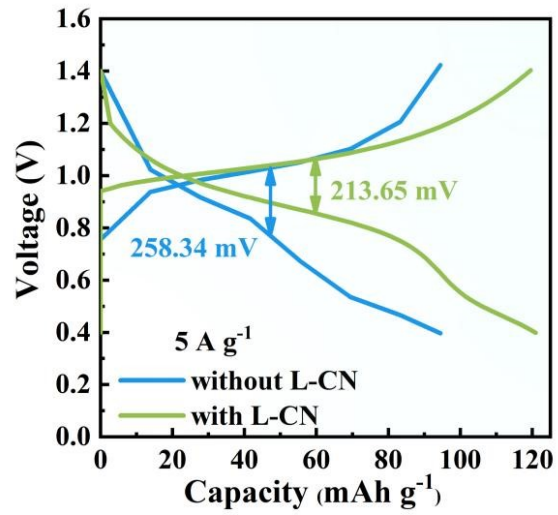


**Figure S30.** The voltage hysteresis of the Zn//V<sub>2</sub>O<sub>5</sub> full cells in electrolytes with/without L-CN additive at 5 A g<sup>-1</sup>.

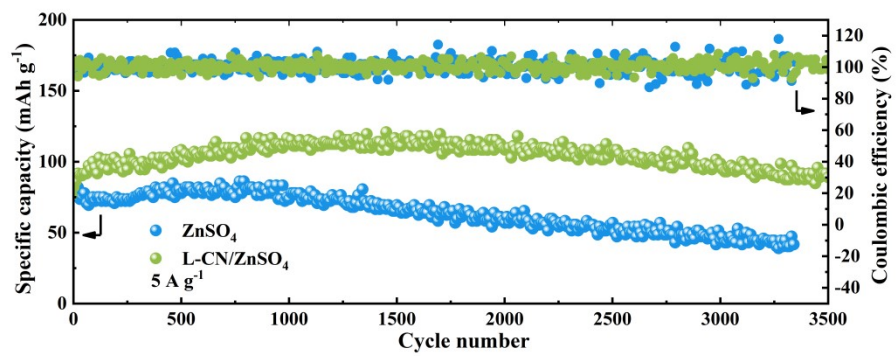


**Figure S31.** Long-term cycling performance of Zn//V<sub>2</sub>O<sub>5</sub> full cells in pure ZnSO<sub>4</sub> and L-CN/ZnSO<sub>4</sub> electrolytes at the current density of 5 A g<sup>-1</sup>.

**Table S1.** Fitting results for symmetric cells at different temperatures.

Symmetrical cells	Res	20°C	30°C	40°C	50°C	60°C
ZnSO <sub>4</sub> electrolyte	R <sub>ct</sub>	2575.0	1061.0	624.7	390.3	219.9
L-CN/ZnSO <sub>4</sub> electrolyte	R <sub>ct</sub>	710.3	389.7	230.7	145.1	115.1

**Table S2.** Performance comparison of Zn half cell using L-CN/ZnSO<sub>4</sub> electrolyte with other reported literatures.

No.	Electrolyte	Current density (mA cm <sup>-2</sup> )	Capacity (mAh cm <sup>-2</sup> )	Cycle number	Average CE (%)	Ref.
<b>1</b>	<b>L-CN/ZnSO<sub>4</sub></b>	<b>5</b>	<b>4</b>	<b>220</b>	<b>98.3</b>	<b>This</b>
		<b>10</b>	<b>1</b>	<b>1000</b>	<b>98.9</b>	<b>work</b>
2	ZHA electrolyte	1	1	300	99.3	[11]
3	Na <sub>4</sub> EDTA additive	0.5	0.5	300	98.4	[2]
4	ZnSO <sub>4</sub> +Arg	1	1	375	98.3	[3]
5	ZnSO <sub>4</sub> +Glucose	1	0.5	200	97.2	[4]
6	ASE	1	1	90	99.9	[5]
7	2 M Zn(OTf) <sub>2</sub>	1	0.5	50	≈100	[6]
8	ZnSO <sub>4</sub> +TA	1	1	150	99.3	[7]
9	PEGDME-50	1	1	100	99.2	[8]
10	ZnSO <sub>4</sub> with NMP 5	1	0.5	1000	99.7	[9]
11	ZnSO <sub>4</sub> with H <sub>3</sub> PO <sub>4</sub>	1	0.5	500	<b>90.0</b>	[10]
12	Zn(TFSI) <sub>2</sub> + Acetamide(1:7)	1	0.5	100	<b>98.5</b>	[11]
13	Zn(ClO <sub>4</sub> ) <sub>2</sub> + NaClO <sub>4</sub>	0.2	0.6	200	<b>98.2</b>	[12]
14	Zn(OTf) <sub>2</sub> +Mn(OTf) <sub>2</sub>	3	1	1170	<b>98.6</b>	[13]
15	BIS-TRIS+ZnSO <sub>4</sub>	5	5	320	<b>98.5</b>	[14]

**Table S3.** Performance comparison of Zn symmetric cell using L-CN/ZnSO<sub>4</sub> electrolyte with other reported literatures.

No.	Electrolyte	Current density (mA cm <sup>-2</sup> )	Capacity (mAh cm <sup>-2</sup> )	Cycle time (hour)	Polarization Voltage (mV)	Ref.
		<b>1</b>	<b>1</b>	<b>6083</b>	<b>26</b>	
<b>1</b>	<b>L-CN/ZnSO<sub>4</sub></b>	<b>8.85</b>	<b>8.85</b>	<b>980</b>	<b>53.7</b>	<b>This work</b>
		<b>40</b>	<b>1</b>	<b>676</b>	<b>126.5</b>	
2	ZHA electrolyte	1	1	1300	40	[1]
3	Na <sub>4</sub> EDTA additive	2	2	450	99	[2]
4	CHAE	1	1	580	51.5	[15]
5	ZnSO <sub>4</sub> +Arg	10	4	≈900	100	[3]
6	Sac/ZnSO <sub>4</sub>	10	10	550	≈80	[16]
7	ZnSO <sub>4</sub> +Glucose	5	5	270	≈75	[4]
8	ASE	1	1	500	≈40	[5]
9	2 M Zn(OTf) <sub>2</sub>	1	0.25	800	42	[6]
10	ZnSO <sub>4</sub> +TA	5	2.5	500	115	[7]
11	ZnSO <sub>4</sub> +TSC	5	1.25	≈210	≈35	[17]
12	PEGDME-50	0.25	0.25	2000	≈130	[8]
13	ZnSO <sub>4</sub> with 18C6	1	1	2400	100	[18]
14	ZnSO <sub>4</sub> with DME	2	2	380	≈120	[19]
15	ZnSO <sub>4</sub> with GQDs	2	0.2	1800	50	[20]
16	ZnSO <sub>4</sub> with 20 DMSO	1	1	2100	128.7	[21]
17	ZnSO <sub>4</sub> with NMP 5	1	1	540	≈54	[9]

---

18	NH <sub>4</sub> OAc additive	10	1	1000	≈70	[22]
19	67Malt/ZS	1	0.5	1200	54.7	[23]
20	ZnSO <sub>4</sub> with H <sub>3</sub> PO <sub>4</sub>	1	0.5	1500	≈30	[10]
21	DME40	10	5	800	≈200	[24]
22	ZnSO <sub>4</sub> with VER	5	5	800	≈112.5	[25]

---

## References

- [1] J. Shi, K. Xia, L. Liu, C. Liu, Q. Zhang, L. Li, X. Zhou, J. Liang, Z. Tao, *Electrochim. Acta* **2020**, 358, 136937.
- [2] S.-J. Zhang, J. Hao, D. Luo, P.-F. Zhang, B. Zhang, K. Davey, Z. Lin, S.-Z. Qiao, *Advanced Energy Materials* **2021**, 11, 2102010.
- [3] H. Lu, X. Zhang, M. Luo, K. Cao, Y. Lu, B. B. Xu, H. Pan, K. Tao, Y. Jiang, *Advanced Functional Materials* **2021**, 31, 2103514.
- [4] P. Sun, L. Ma, W. Zhou, M. Qiu, Z. Wang, D. Chao, W. Mai, *Angew. Chem. Int. Ed.* **2021**, 60, 18247.
- [5] Q. Zhang, Y. L. Ma, Y. Lu, X. Z. Zhou, L. Lin, L. Li, Z. H. Yan, Q. Zhao, K. Zhang, J. Chen, *Angew. Chem. Int. Ed.* **2021**, 60, 23357.
- [6] D. Yuan, J. Zhao, H. Ren, Y. Chen, R. Chua, E. T. J. Jie, Y. Cai, E. Edison, W. Manalastas, Jr., M. W. Wong, M. Srinivasan, *Angew. Chem. Int. Ed.* **2021**, 60, 7213.
- [7] J. Cao, D. Zhang, R. Chanajaree, Y. Yue, Z. Zeng, X. Zhang, J. J. A. P. M. Qin, *Adv. Powder Mater.* **2022**, 1, 100007.
- [8] Z. Hou, Z. Lu, Q. Chen, B. Zhang, *Energy Stor. Mater.* **2021**, 42, 517.
- [9] T. C. Li, Y. Lim, X. L. Li, S. Luo, C. Lin, D. Fang, S. Xia, Y. Wang, H. Y. Yang, *Adv. Energy Mater.* **2022**, 12, 2103231.
- [10] Y. Liu, J. Hu, Q. Lu, M. Hantusch, H. Zhang, Z. Qu, H. Tang, H. Dong, O. G. Schmidt, R. J. E. S. M. Holze, *Energy Stor. Mater.* **2022**, 47, 98.
- [11] H. Qiu, X. Du, J. Zhao, Y. Wang, J. Ju, Z. Chen, Z. Hu, D. Yan, X. Zhou, G. J. N. c. Cui, *Nat. Commun.* **2019**, 10, 5374.
- [12] Y. Zhu, J. Yin, X. Zheng, A.-H. Emwas, Y. Lei, O. F. Mohammed, Y. Cui, H. N. J. E. Alshareef, E. Science, *Energy Environ. Sci.* **2021**, 14, 4463.
- [13] H. He, J. J. J. o. M. C. A. Liu, *J. Mater. Chem. A* **2020**, 8, 22100.
- [14] M. Luo, C. Wang, H. Lu, Y. Lu, B. B. Xu, W. Sun, H. Pan, M. Yan, Y. Jiang, *Energy Stor. Mater.* **2021**, 41, 515.
- [15] B. W. Olbasa, C. J. Huang, F. W. Fenta, S. K. Jiang, S. A. Chala, H. C. Tao, Y. Nikodimos, C. C. Wang, H. S. Sheu, Y. W. Yang, T. L. Ma, S. H. Wu, W. N. Su, H. Dai, B. J. Hwang, *Adv. Funct. Mater.* **2021**, 32, 2103959.
- [16] C. Huang, X. Zhao, S. Liu, Y. Hao, Q. Tang, A. Hu, Z. Liu, X. Chen, *Adv. Mater.* **2021**, 33, 2100445.
- [17] N. Wang, S. Zhai, Y. Ma, X. Tan, K. Jiang, W. Zhong, W. Zhang, N. Chen, W. Chen, S. Li, G. Han, Z. Li, *Energy Stor. Mater.* **2021**, 43, 585.
- [18] R. Li, M. Li, Y. Chao, J. Guo, G. Xu, B. Li, Z. Liu, C. J. E. S. M. Yang, *Energy Stor. Mater.* **2022**, 46, 605.
- [19] J. Cui, X. Liu, Y. Xie, K. Wu, Y. Wang, Y. Liu, J. Zhang, J. Yi, Y. Xia, *Mater. Today Energy* **2020**, 18, 100563.
- [20] H. Zhang, R. Guo, S. Li, C. Liu, H. Li, G. Zou, J. Hu, H. Hou, X. Ji, *Nano Energy* **2022**, 92, 106752.
- [21] D. Feng, F. Cao, L. Hou, T. Li, Y. Jiao, P. J. S. Wu, *Small* **2021**, 17, 2103195.
- [22] D. Han, Z. Wang, H. Lu, H. Li, C. Cui, Z. Zhang, R. Sun, C. Geng, Q. Liang, X. J. A. E. M. Guo, *Adv. Energy Mater.* **2022**, 12, 2102982.

- [23] W. Chen, S. Guo, L. Qin, L. Li, X. Cao, J. Zhou, Z. Luo, G. Fang, S. J. A. F. M. Liang, *Adv. Funct. Mater.* **2022**, 32, 2112609.
- [24] G. Ma, L. Miao, Y. Dong, W. Yuan, X. Nie, S. Di, Y. Wang, L. Wang, N. J. E. S. M. Zhang, *Energy Stor. Mater.* **2022**, 47, 203.
- [25] M. Qiu, L. Ma, P. Sun, Z. Wang, G. Cui, W. J. N.-M. L. Mai, *Nanomicro Lett.* **2022**, 14, 31.